Risk Assessment Method of Industrial Urban Areas Considering Building Vulnerability

Wenling Guan*, Yutong Wang, Chengjie Dong
School of Environmental Science and Safety Engineering, Tianjin University of Technology, Tianjin, China
**Corresponding Author.*

Abstract: **Industrial accidents may result in injuries and damage to buildings. Buildings as an important category of hazard-bearing bodies in industrial accidents cannot be ignored in regional risk assessment. The purpose of this study is to introduce building vulnerability into the study of hazard-bearing body vulnerability and build a comprehensive vulnerability assessment model of hazard-bearing body. A comprehensive risk assessment method is proposed which considers the accident consequences and the vulnerability of hazard-bearing body. Firstly, an accident scenario was established and accident footprints were spatially displayed using the hazard modeling software ALOHA. Secondly, the building vulnerability is evaluated based on the exposure, sensitivity and adaptability of the buildings. Building density and distance from the accident center are selected into the exposure index layer. Building age, building height, seismic grade of building are selected into the sensitivity index layer. Emergency shelter area and road area are selected into the adaptability index layer. Finally, ArcGIS is used to superimpose accident consequence map and hazard-bearing body vulnerability map to generate comprehensive risk map and realize regional comprehensive risk visualization. This procedure was tested in a small town in China, and the results showed that the inclusion of building vulnerability in the risk assessment system led to more accurate results.**

Keywords: Building Vulnerability; Hazard Footprint; Composite Risk Map; Risk Assessment.

1. Introduction

As industrialization accelerates, so do the social risks associated with it. Fire and explosion accidents caused by industrial hazardous sources have occurred from time to time. For example, the 2010 explosion at a petrochemical company's tank farm in Lanzhou, China, shattered windows and doors of houses within 1.7 kilometers and tremors were felt within 20 kilometers, resulting in six deaths and six injuries. In 2015, a particularly major fire and explosion occurred at the Ruihai Company's dangerous goods containers in the port of Tianjin, China, killing 165 people and collapsing more than 300 surrounding buildings. In 2020, a massive explosion caused by the ignition of ammonium nitrate in the port of Beirut, Paris, resulted in 190 deaths, more than 6,500 injuries, 300, 000 people left homeless, and more than 50,000 buildings damaged. As can be seen from the above cases, industrial accidents not only cause a large number of casualties but also damage to nearby buildings. Therefore, an accurate assessment of the risk of accidents that may be caused by industrial hazards is necessary. This will help city managers to make safe land-use planning and thus reduce possible social risks. As early as the 1970s, some countries began to use regional quantitative risk assessment methods to study safety land-use planning near industrial parks. The 1984 Bhopal accident in India further raised the awareness of highly hazardous facilities and their surrounding land-use. Following the enactment of the Directive, many scholars have explored regional risk assessment methodologies. Hauptmanns [1] proposed a risk-based framework for calculating appropriate distances between industrial facilities and residents in Germany’s industrial zones. Li [2] introduced a technique for risk identification, management, and land-use planning that was based on population vulnerability. Rajeev [3] developed

risk assessment models using geographic information tools to assess the level of population vulnerability and hazards caused by chemical accidents and hazardous materials rail transportation. Existing studies on regional risk assessment have focused more on human and neglected buildings (another typical hazard-bearing body in accidents). This may lead to inaccurate risk assessment results. Therefore, this study proposed a risk assessment model considering the vulnerability of buildings based on previous studies.

Current research on building vulnerability focuses more on the area of natural hazards (*e.g.*, mudslides, landslides, floods, and earthquakes). The assessment approaches include expert judgment, statistical analysis of historical damage data, and physically based numerical simulation analyzed the operational behavior of landslides using a depth-averaged model and evaluated the damage degree of buildings under landslide impacts by the finite element method. For the evaluation of building vulnerability caused by flood hazards, many studies have used evaluation methods based on historical flood data. Some scholars evaluated building vulnerability to flooding by analyzing building characteristics gathered from big data. Englhardt [4] developed a large-scale flood vulnerability assessment method based on the fine-scale ImageCat dataset. Some researchers who focus on developing building vulnerability functions under flood hazards. For building vulnerability assessment under seismic hazard, some scholars have constructed vulnerability functions for different types of building structures based on seismic hazard data or numerical simulations to obtain damage probability matrices or vulnerability curves. In Italy, Iran, Portugal and other countries, empirical data have been effectively utilized to validate and develop new seismic vulnerability assessment frameworks. To accomplish the regional rapid seismic vulnerability assessment of buildings, the index approach is also utilized to evaluate the building vulnerability. Italian scholars established different physical vulnerability assessment index systems for masonry and reinforced concrete structures based on expert judgment and the seismic characteristics of buildings (National Group for Earthquake Protection, GNDT I and II). Several scholars (*e.g.*, Refs. [5-7]) have analyzed the structural characteristics of buildings on the basis of this methodology and proposed a new indicator system for adapting to different building structure types.

As can be seen from the studies above, little consideration has been given to the vulnerability of buildings caused by industrial accidents. Accordingly, this paper proposed a methodology for assessing building vulnerability caused by industrial accidents and introduced building vulnerability into the vulnerability assessment model of hazard-bearing body. On this basis, overlaying the consequences of regional industrial accidents, the regional risk was graded to form different risk levels. The results can help urban planning and management departments to understand regional risk and establish a scientific foundation for urban land and emergency material planning.

2. Methodology

The CR assessment procedure is illustrated in Figure 1. Firstly, the building vulnerability indicators were identified, and the AHP-entropy weighting methodology was utilized to determine the weights of the indicators. Vulnerability maps of the hazard-bearing body (including population and buildings) were created. ALOHA was used to create accident scenarios and simulate hazard footprints in the case study area, which were then overlaid on satellite maps to visualize and characterize the consequences of the accidents using ArcGIS. Finally, the industrial hazard maps were overlaid with the vulnerability maps of the hazard-bearing body to generate a comprehensive regional risk map.

2.1 Gridding of the Research Area

First, the research area was determined, and the boundaries of the study area were identified and demarcated using satellite maps to determine the distribution of buildings. Subsequently, field surveys were performed to collect data on local buildings, population distribution and weather conditions. Gridding is the basis of CR mapping. Li [2] partitioned a 20 km × 20 km study area into a grid with dimensions of 500 m × 500 m. Tahmid [8] set the grid size to 0.1mile × 0.1mile. Too large a grid can not accurately reflect the risk distribution, and too small a grid will ignore

the spatial correlation between adjacent evaluation units, so the grid should be delineated by the actual situation of the research area to ensure that each grid is uniform. In this study, the area was divided into 400 m × 400 m grid cells.

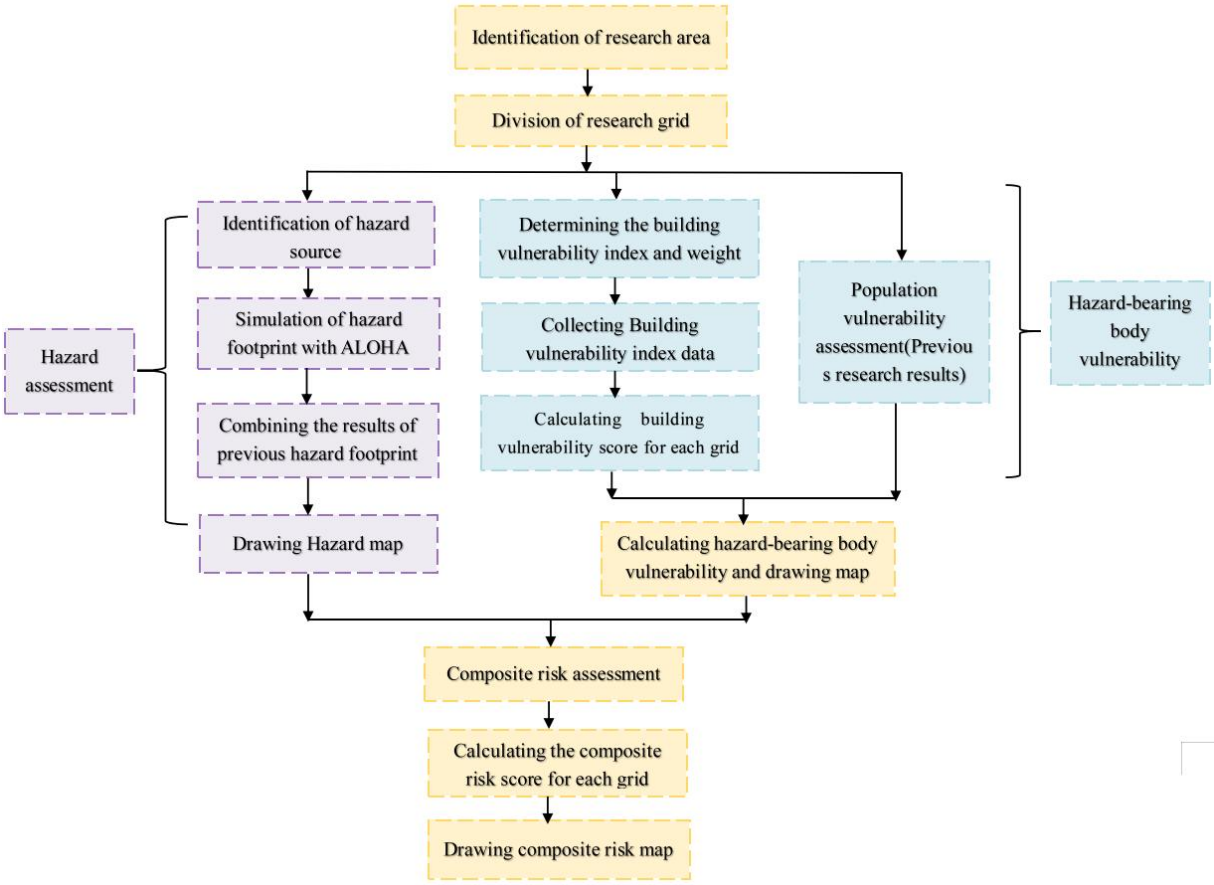

Figure 1. CR Assessment Procedure.

2.2 Building Vulnerability Assessment

2.2.1 Determine building vulnerability indicators.

Vulnerability refers to the characteristics of objects that are vulnerable, susceptible to injury and damaged. The concept of vulnerability first originated from the study of natural disasters, and then was widely used in other disciplines, including geography, engineering, environmental science, sociology, etc. With the outreach of the connotation of vulnerability research, vulnerability evaluation models have also been continuously improved and developed. The VSD model was first developed by [9] based on the ESA (Exposure-Sensitivity-Adaptability) model, which considers that the vulnerability consists of exposure, sensitivity and adaptive capacity, and builds the model step-by-step through the central, dimensional, indicator, and parameter layers. The model has been widely used because of its clear meaning and standardized assessment process. Therefore, this study adopted the VSD model to construct the building vulnerability evaluation index system. Evaluation indicator selection is the basis for constructing the indicator model. The selection of building vulnerability indicators in this study follows the principles of scientific, representativeness, independence, systematicity, operability, and ease of quantification. Based on the pieces of literature, the characteristics of urban buildings and the types of injuries caused by industrial accidents, indicators of building vulnerability were identified.

Exposure refers to the degree of unfavourability of the hazard-bearing body to external pressure or coercion, where the extent of the influence of the causative factor and the spatial location of the hazard-bearing body are the main influences on the degree of exposure. In the event of an industrial accident, immediate attention should be given to densely built-up areas and buildings near the accident

center. Areas with high building density such as commercial and residential areas must be prioritized in the emergency response plan. Therefore, building density and distance from the accident center were included in the exposure dimension layer.

Sensitivity refers to the degree of response of the hazard-bearing body to industrial accident disturbances, which is determined by the nature of the hazard-bearing body itself, including the natural characteristics of the hazard-bearing body as well as the social characteristics. The structural design of the building and the materials used will directly affect its ability to withstand the blast, such as steel structure can withstand the pressure of the shock wave better than concrete structure; old buildings or unmaintained buildings may be more vulnerable to damage in the explosion; under the action of the shock wave, the high-rise buildings may undergo serious deformation, damage or even collapse. Therefore, building age, building height, and seismic grade of building were included in the sensitivity dimension layer.

The capacity of a system to return to its usual condition following disturbance is referred to as adaptability. This suggests that building vulnerability after an accident is significantly influenced by the level of resource access to buildings surrounding the industrial park. Therefore, emergency shelter area and road area were selected to the adaptability dimension layer.

The final building vulnerability evaluation index system is shown in Figure 2**.**

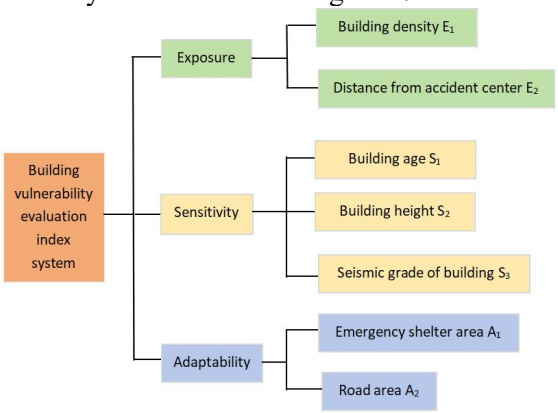

Figure 2. Building Vulnerability Assessment Index System

2.2.2 Calculation of building vulnerability

Each indicator is designed to reflect the characteristics of building vulnerability in different aspects, so there will be inconsistencies in the outline of each data, and the size of the value is very different, in order to unify the calculation and evaluation, it is necessary to carry out reasonable standardized processing of raw data [10]. According to the nature of the evaluation indicators, the specific indicators are divided into two categories: positive and negative, which are standardized separately:

Positive parameter: the larger the value, the higher the vulnerability (e.g. building density). The corresponding functional expression is given in Eq. (1)

$$X_i = \frac{x_i - x_0}{x_0} = \begin{cases} \frac{x_i - x_0}{x_0} & x_i > x_0 \\ 0 & x_i \le x_0 \end{cases} \quad (1)$$

Negative parameter: the larger the value, the lower the vulnerability (e.g. seismic grade of the building). The corresponding function expression is given in Eq. (2)

$$X_i = \frac{x_0 - x_i}{x_0} = \begin{cases} \frac{x_0 - x_i}{x_0} & x_i > x_0 \\ 0 & x_i \le x_0 \end{cases} \quad (2)$$

In the above function, X_i is the dimensionless value of x_i among the parameters of the vulnerability indicator, reflecting the dispersion of all parameters included in the concept of vulnerability; x_i is the statistical value of parameter i; and x_0 is the standard value of parameter i. Through the above process, t the raw data for all indicators are standardized. The vulnerability calculation methodology is based on the Dhaka Profile and Earthquake Risk Atlas [11]. Building vulnerability scores were calculated as follows.

$$BVS(x,y) = \sum_{i=1}^{7} IW_i \cdot IX_i \quad (3)$$

$BVS_{(x,y)}$—building vulnerability score at grid coordinates (x,y).

IW_i— the weight coefficient of the ith index

$IX_{i,\,(x,y)}$—the quantitative index score of the ith index at the grid coordinate (x,y).

Eq. (3). was utilized to determine the BVS values of every grid cell within the research region. They all have values between 0 and 1. A higher score indicates that the grid cell's building vulnerability is greater, and the buildings are more vulnerable to accidents.

2.2.3 Determination of indicator weights

Weight calculation methods can be roughly classified into two categories: subjective judgment method and objective assignment method, which are widely used in multi-objective decision-making problems and

comprehensive evaluation problems of complex systems. Subjective judgment methods, such as hierarchical analysis, assign weights to each indicator according to the judgment of subjective experts, decision-makers and different stakeholders. However, it lacks stability and universal applicability because it relies too much on experts' subjective judgments. The objective assignment method is a quantitative analysis method, such as the entropy value method and principal component analysis; it is based on the information of indicator data and calculates the weight coefficients by establishing certain mathematical and theoretical derivation, but it ignores the subjective intentions of decision-makers, and there will be instances where the weights assigned are not in line with the relative importance of the attributes. Therefore, the combined assignment method using hierarchical analysis-entropy weighting helps decision-makers evaluate the current status of the indicator system fairly and objectively. The AHP-entropy weight methodology was used to quantify the weights of building vulnerability indicators in this paper.

2.2.4 Mapping of the hazard-bearing body vulnerability

When industrial hazards cause accidents, population vulnerability and building vulnerability combine to influence the consequences of accidents. The population vulnerability score (PVS) adopts the research results of [12]. Given that the BVS and PVS values range from 0 to 1, the vulnerability of each grid cell in the region can be calculated by dividing the above hazard-bearing body vulnerability score into different levels using Table 1. This study used ArcGIS software to create a hazard-bearing body vulnerability map of the area to depict the spatial distribution characteristics of building and population vulnerability in the research area, and grid cells were colored to show the vulnerability of different hazard bodies.

Table 1. Range for Different Levels of Building and Population Vulnerability

PVS/BVS value	Building/Population vulnerability level
$0.75 \leqslant BVS_{(x,y)}/PVS_{(x,y)} \leqslant 1$	Seriously vulnerable
$0.5 \leqslant BVS_{(x,y)}/PVS_{(x,y)} < 0.75$	High vulnerable
$0.25 \leqslant BVS_{(x,y)}/PVS_{(x,y)} < 0.5$	Quite vulnerable
$0 < BVS_{(x,y)}/PVS_{(x,y)} < 0.25$	A bit vulnerable
$BVS_{(x,y)}/PVS_{(x,y)} = 0$	No vulnerable

After the accident occurred, regions where two vulnerabilities overlap face higher risk. Based on the spatial characteristics of the hazard-bearing body by the same unit, the results of population vulnerability and building vulnerability assessments can be summarized by a risk matrix, as shown in Table 2.

Table 2. Hazard-bearing Body Vulnerability Risk Matrix

Building / Population	Seriously vulnerable	High vulnerable	Quite vulnerable	A bit vulnerable	No vulnerable
Seriously vulnerable	Very seriously	Seriously	Seriously	Seriously	Seriously
High vulnerable	Seriously	Seriously	High	High	High
Quite vulnerable	Seriously	High	High	Quite	Quite
A bit vulnerable	Seriously	High	Quite	A bit	A bit
No vulnerable	Seriously	High	Quite	A bit	No vulnerable

2.3 Hazard Assessment

2.3.1 Hazard identification

Accidents are mostly caused by hazards. Conducting field surveys of the study area, basic information on regional hazard sources is obtained involved in the composition of hazardous substances, storage methods, storage conditions, storage quantities and so on. etc.

2.3.2 Hazard footprint simulation

After identifying hazards, based on the principle of maximum risk, the accidents that result in the most damage to the

hazard-bearing body were chosen for hazard footprint simulation. To identify hazardous areas and draw hazard maps, ALOHA software is used to simulate the extent of the accident. The level of concern (LOC) is the threshold of the hazard. Various levels of toxic concentration, explosive pressure, or thermal radiation threat correspond with distinct LOCS. Threat areas can be overlaid on satellite maps to depict the hazard footprint spatially.

2.3.3 Hazard map drawing

According to ALOHA hazard footprint simulation, Guan [12] superimposed the hazard footprint into the study grid, which can clearly show the degree of accident hazards in different grid areas. The hazard footprint in this research was mapped using this technique. Hazard footprints were categorized into different LOC levels based on the scope and severity of the hazard. When one threatened region overlaps with another, the most hazardous threatened area determines the overlapped area. As a result, its hazard level is set to the highest level of the two overlapped zones. This technique determined each grid cell's degree of hazard, and the accident risk map for the region was created using ArcGIS to visualize the severity of the accident consequences in each grid cell and prepare the following drawing of the CR map.

2.4 CR Assessment

2.4.1 Calculation of CR

This study created a comprehensive risk assessment method by taking potential industrial accident consequences into account and the vulnerability of hazard-bearing bodies in the vicinity of the accident center. In this paper, building vulnerability is considered. Based on the results of the assignments in the previous sections, each grid cell displays its vulnerability level and accident risk level it carries, and the CR score for each grid is determined according to Eq. (4).

$$CR_{(x,y)} = function\left(LOC_{(x,y)}, V_{(x,y)}\right) \quad (4)$$

$CR_{(x,y)}$—the score of CR at map coordinates (x, y).

$LOC_{(x,\ y)}$—hazard level at map coordinates (x, y).

$V_{(x,\ y)}$—the score of hazard-bearing body vulnerability at map coordinates (x, y).

Following the hazard assessment, there were four levels of hazards: LOC3, LOC2, LOC1 and no hazard. When threat regions overlap, the worst scenario is considered, e.g., if LOC2 for an accident scenario and LOC3 for another scenario overlap each other in a grid cell, the hazard level for that grid cell will be LOC3, representing the worst scenario. The vulnerability score of the hazard-bearing body for each grid cell was classified into five levels: Very seriously, high, quite, a bit and no vulnerable. According to the risk matrix shown in Table3, each element in this matrix represents a CR score based on the combined effect of hazard and vulnerability levels.

The CR score is classified as “medium” between high and low if the hazard level is LOC1 and the corresponding V is “High”. If the hazard class is LOC2 and the corresponding V is “High”, the CR score is “High” because there is no classification between “high” and “medium”. Consequently, the risk level is determined by identifying which of the two is more dangerous. Furthermore, vulnerability and hazard influence risk. If a grid cell has V=0 (no hazard-bearing body, the CR score for that grid cell is “no risk” regardless of the accident hazard level, and the same is true if the accident hazard level is “no risk”. Finally, grid cells were categorized into six levels: Serious high, very high, high, medium, low and no risk.

Table 3. Risk Matrix

Hazard level / Hazard-bearing body vulnerability	LOC4	LOC3	LOC2	LOC1	No hazard
Very high	Serious high	Very high	Very high	High	No risk
High	Very high	Very high	High	Moderate	No risk
Moderate	Very high	High	High	Moderate	No risk
Low	High	Moderate	Moderate	Low	No risk
No hazard	No risk	No risk	No risk	No risk	No risk

2.4.2 CR map drawing

Finally, ArcGIS fishnet's assignment function was used to assign CR values to each grid unit using colors ranging from light to dark to signify increasing risks in sequence. The CR map illustrates the spatial distribution of

hazard and hazard-bearing body vulnerability and serves as a foundation for town area planning, emergency deployment, and resettlement of people living in these damaged buildings.

3. Case Studies

Population vulnerability in this case cites the authors' previous findings for Guan [12], this section emphasizes the assessment of building vulnerability.

3.1 Select and Divide the Research Area

This study was conducted in Town C of Tianjin, China, which has a town area of 93 square kilometers and a total population of 42,000 people. It has 24 administrative villages and 2 industrial parks under its jurisdiction. There are about 15,675 buildings in the town, of which 324 are residential. According to the meteorological data in recent years, the town's year-round dominant wind direction is southwest. As a town with Chinese characteristics, Town C has been experiencing rapid economic development in recent years, with many enterprises settling here, and there are 594 industrial enterprises in Town C. These industrial enterprises drive the economic development of Town C and also increase the potential risk of accidents in the town. The research area was separated into 491 grid cells, each measuring 400 m × 400 m for further analysis.

3.2 Data Acquisition

3.2.1 Analysis of building vulnerability objectives

Through the field survey and ArcGIS vector data processing, the types of building structures in the town were categorized into steel structure, reinforced concrete structure, brick-concrete structure, and frame structure. The specifics are shown in Table 4.

Table 4. Type of Building Structure in Town C

Serial number	Type of building structure	Proportion
1	Brick-concrete structure	62.8%
2	Steel structure	30.2%
3	Frame structure	3.7%
4	Reinforced concrete structure	3.3%

3.2.2 Analyzing the major hazard sources

In the town, there are 33 hazardous chemical production and storage businesses. There are many enterprises engaged in the production, operation, and storage of hazardous chemicals in Town C, including 66 hazardous chemicals in all, such as kerosene, gasoline, crude oil, and heavy aromatic hydrocarbons. Among them, the leakage of crude oil can easily evaporate and form combustible gases, which can cause explosions. In the event of an accident, it may lead to serious building damage. In this study, according to the principle of maximum risk, 6 hazardous substances from 13 hazardous chemical enterprises were selected to simulate hazard footprint as shown in Table 5.

Table 5. Hazardous Chemical Enterprises in Town C.

Number	Hazardous chemicals	Hazard category	Annual consumption (ton/ year)
1	Solvent oil	Flammable liquid	8504
2	Naphtha	Flammable liquid	1842
3	Gasoline	Flammable liquid	171730
4	Petrol	Flammable liquid	3199225
5	Crude oil	Flammable liquid	2100000
6	Heavy aromatics	Flammable liquid	8000

3.3 Hazard Assessment

Based on the results of hazard identification, hazard ranges were simulated by ALOHA, and the influence area of accident consequences was classified according to the spatial footprint. Shockwave overpressure from explosions is the most damaging to buildings. So, the TNT equivalent calculation model and shock wave hazard radius formula were chosen to simulate the consequences of hazard source accidents. For modeling chemical releases, this study used ALOHA's preferred Acute Exposure Guideline Levels (AEGLs) as shock wave overpressure LOCS in the simulation of Oil and other storage tank leak. The simulation results as shown in Figure 3. and Figure 4**.** The threat zones with red reveal the most severe hazard level. In this zone, the building will be destroyed and collapsed; the threat zones with

orange denote cracks in the walls and yellow threat zones indicate damaged windows and doors. In hazard mapping, the hazard footprints were categorized into four types. LOC1 indicates the lowest hazard level, LOC2 and LOC3 indicate progressively higher levels, in that order, indicate a higher level of hazard. The shockwave hazard footprint, combined with the hazard footprint of the toxic spill from Guan [12], was used to create a hazard map, as shown in Figure 5, to visualize the impacted region and the consequences of the accident. The hazard level of a grid cell that is covered by the hazard footprints of both accidents is determined by the more hazardous level of the two. If a grid cell has a hazard level of LOC3 for both types of accidents, the grid hazard level is set to LOC4. The hazard map was drawn using ArcGIS (seen in Figure 6.). The grid cells with darker colors have more serious consequences of accidents than those with lighter colors.

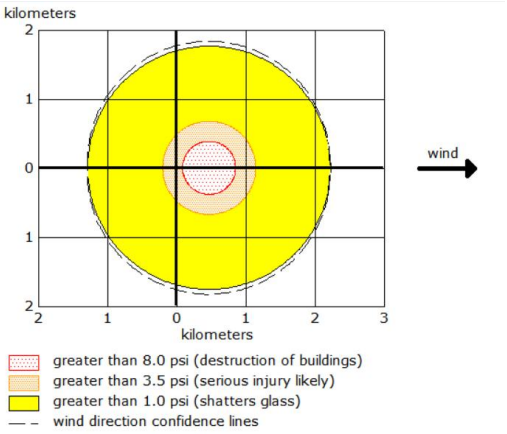

Figure 3. Damage Range of Crude Oil Leakage Vapor Cloud Explosion Shock Wave

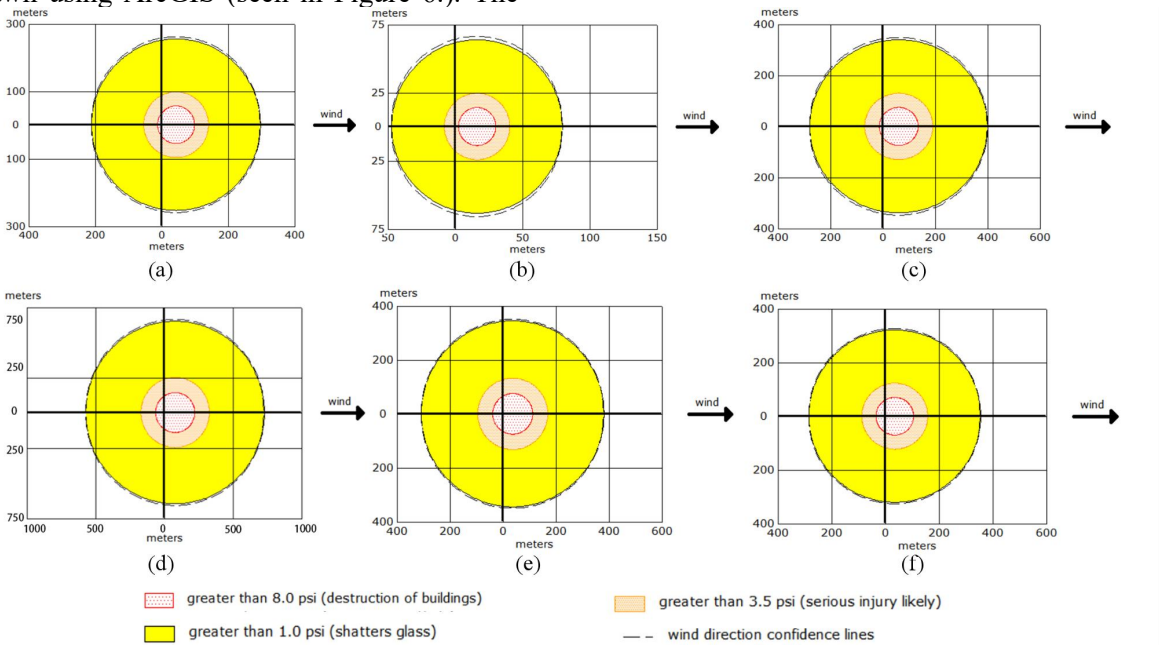

Figure 4. Storage Tank Leakage Hazard Footprint for (a)500m³ Naphtha (b)500m³Ammonia (c)1000m³Solvent Oil (d)2000m³Paraffin (e)1250m³Heavy Aromatics(f)1000m³Heavy Aromatics

3.4 Assessment of the Hazard-bearing Body Vulnerability

The results of the combined AHP-entropy weight method calculations are shown in Table6. Building data for this study were obtained from vectorization of the building map information of the study area through a 0.5 m resolution satellite map. The data information was further updated and verified through field visits, and the vector data model was stored in the GIS database. The results of calculating the weights of the building and population vulnerability indicator system are shown in Table 7.

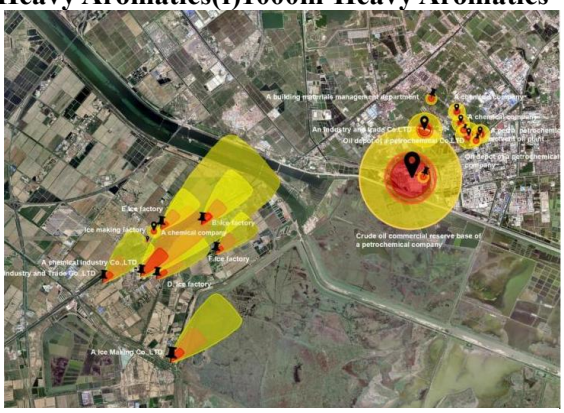

Figure 5. The Footprint of Hazards in Terms of Space

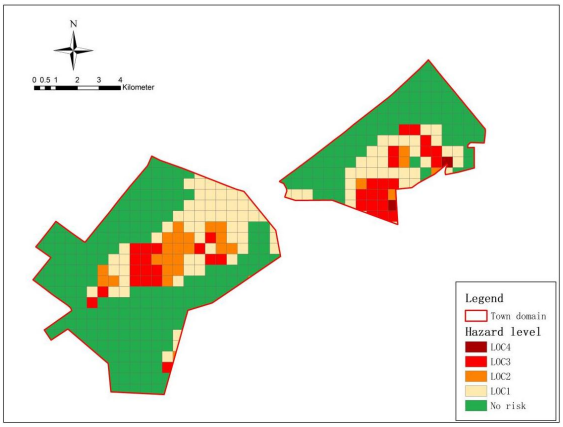

Figure 6. Hazard Map

Table 6. The Revised AHP, Entropy Weight Method and Combined Weight Calculation Results

Indicator layer	AHP W_1	Entropy W_2	Combined weight W
Building density	0.139	0.249	0.194
Distance from accident center	0.190	0.121	0.155
Building age	0.127	0.071	0.099
Building height	0.176	0.174	0.175
Seismic grade of building	0.204	0.263	0.234
Emergency shelter area	0.066	0.087	0.076
Road area	0.098	0.035	0.067

Table 7. Building Vulnerability Assessment Index

Target layer	Criterion layer	Weight
Vulnerability of building	Building density	0.194
	Distance from the center of accident	0.155
	Building age	0.099
	Building height	0.175
	Seismic grade of building	0.234
	Emergency shelter area	0.076
	Road area	0.067

The level of building and population vulnerability indicators was initially determined for each grid cell, and then the hazard-bearing body vulnerability level was calculated through the risk matrix. As shown in Figure 7, the vulnerability levels were connected to the grid cells using ArcGIS software, and their spatial distribution was shown by different colors. The towns in the east are more vulnerable than the ones in the west, as Figure 7. illustrates. This is owing to a concentration of residential areas in the eastern towns with highly sensitive areas for the population such as old people's homes and kindergartens; at the same time, the eastern region has more rural self-built houses with brick-concrete structures and longer age of the buildings, which make the vulnerability of hazard-bearing bodies higher in the eastern towns. In contrast, the western town has many industrial parks and residences that are located close to National Highway 205. Local building vulnerability is significantly reduced by sparse buildings and convenient transportation. The introduction of building vulnerability makes the results of vulnerability assessments more realistic than considering population vulnerability.

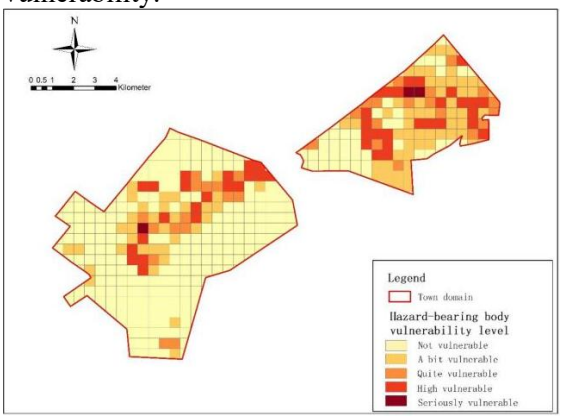

Figure 7. Vulnerability Map of Hazard-Bearing Body

3.5 CR Assessment

Figure 8. CR Map

The CR rank matrix of each grid cell was calculated using risk as shown in Table 4, and the CR map was drawn using ArcGIS software as shown in Figure 8. Compared to previous studies, the number of risk grids in eastern towns increased, and the introduction of building vulnerability made the urban risk assessment results more accurate. Comparing CR Map 8 and Risk Map 6, it is

clear that high hazard zones do not always correspond to high risk. For example, on the hazard map, the eastern part of the town, in the vicinity of the hazard release point, is the most hazardous area (seen in Figure 6), but due to the low vulnerability of the hazard-bearing bodies in the area around the hazard release point, it is categorized as moderate risk on the risk map (seen in Figure 8). This is because CR map is essentially a spatial overlay of hazard and vulnerability maps, which considers hazard and vulnerability simultaneously [2]. The hazard-bearing body vulnerability-based risk analysis methodology provides more a comprehensive perspective of future plant location and emergency management. Relevant departments should establish an effective hazard control system and strengthen the safety management of hazard sources, such as maintaining a reasonable safety distance between residential areas and hazardous sources, relocating hazardous material storage tanks away from buildings, allocating reasonable medical resources and accessible transportation routes to residents.

4. Conclusion

On the basis of the original population vulnerability assessment, this study introduced the building vulnerability study, an integrated vulnerability model of regional hazard-bearing bodies was constructed, and a methodology for risk assessment of urban areas based on industrial accidents was developed with the help of ArcGIS.

The ALOHA software was used to assess the hazard level of the accidental release of specific chemical substances. Seven indicators, such as building density, building height, building age, and seismic grade, were selected and classified into three dimensions, exposure, sensitivity, and adaptability. The AHP-entropy weighting method was used to calculate the weighting values, determine the vulnerability score of each grid, and combine the results of the population vulnerability assessment to generate a comprehensive vulnerability map of the hazard-bearing bodies. The geospatial tools in the ArcGIS were used to draw hazard maps and vulnerability maps of hazard-bearing bodies, which were superimposed to obtain the CR maps. The CR map spatially demonstrates the risks faced by hazard-bearing bodies in towns and cities, which provides management with a visual tool to help them consider potential risks when making decisions. This is particularly important for emergency preparedness, resource allocation and strategic planning.

Comprehensive risk assessments can be used as a decision-making tool for emergency management in areas surrounding industrial zones and land-use planning for new factory sites. Although the study was conducted in only one small town in Tianjin, the methodology applies to the entire region as well as other parts of the city, providing scientific guidance for mitigating the risk of explosion accidents and helping decision-makers better allocate resources and develop contingency plans.

There are also some limitations in this study. The building GIS data were obtained based on fieldwork and ArcGIS vector data processing, and more accurate assessment results can be obtained in the future with the gradual improvement of the information-sharing mechanism among government departments. The CR assessment was conducted based on the current situation in the study area and did not consider future changes in risk. In addition, the risk assessment did not consider the influence of dynamic factors. Some data may change at times, such as building density, emergency shelter area and road area. Therefore, in further research, the risk assessment model should be integrated with software development to create real-time risk analysis software.

References

[1] Hauptmanns U, A risk-based approach to land-use planning, Journal of Hazardous Materials, 2005;125: 1-9.

[2] Li F, Bi J, Huang L, Qu C, Yang J, Bu Q, Mapping human vulnerability to chemical accidents in the vicinity of chemical industry parks, Journal of Hazardous Materials, 2010; 179: 500-06.

[3] Rajeev K, Soman S, Renjith VR, George P, Human vulnerability mapping of chemical accidents in major industrial units in Kerala, India for better disaster mitigation, International Journal of Disaster Risk Reduction, 2019; 39.

[4] Englhardt J, de Moel H, Huyck CK, de Ruiter MC, Aerts J, Ward PJ,

Enhancement of large-scale flood risk assessments using building-material-based vulnerability curves for an object-based approach in urban and rural areas, Natural Hazards and Earth System Sciences, 2019; 19: 1703-22.

[5] Franch KAG, Morbelli GMG, Inostroza MAA, Gori RE, A seismic vulnerability index for confined masonry shear wall buildings and a relationship with the damage, Engineering Structures, 2008;30: 2605-12.

[6] Ferreira TM, Vicente R, da Silva J, Varum H, Costa A, Seismic vulnerability assessment of historical urban centres: case study of the old city centre in Seixal, Portugal, Bulletin of Earthquake Engineering, 2013; 11: 1753-73.

[7] Formisano A, Chieffo N, Marius M, Landolfo R, SEISMIC VULNERABILITY AND DAMAGE OF A HISTORICAL CENTRE IN THE DISTRICT OF CASERTA (ITALY), 2017.

[8] Tahmid M, Dey S, Syeda SR, Mapping human vulnerability and risk due to chemical accidents, Journal of Loss Prevention in the Process Industries, 2020; 68.

[9] Polsky C, Neff R, Yarnal B, Building comparable global change vulnerability assessments: The vulnerability scoping diagram, Global Environmental Change-Human and Policy Dimensions, 2007; 17: 472-85.

[10] Xiu CL, Cheng L, Song W, Wu W, Vulnerability of large city and its implication in urban planning: A perspective of intra-urban structure, Chinese Geographical Science, 2011; 21: 204-10.

[11] Bank W, Dhaka Profile and Earthquake Risk Atlas 2014.

[12] Guan WL, Liu QW, Dong CJ, Risk assessment method for industrial accident consequences and human vulnerability in urban areas, Journal of Loss Prevention in the Process Industries, 2022; 76.

